SAND2020-5032J

Electric-field imaging using polarized neutrons

Yuan-Yu Jau*
Sandia National Laboratories, Albuquerque, NM 87123, USA

Daniel S. Hussey, Thomas R. Gentile, and Wangchun Chen
National Institute of Standards and Technology (NIST), Gaithersburg, MD 20899, USA

(Dated: May 11, 2020)

We experimentally demonstrate, for first time, that electrically neutral particles, neutrons, can be used to directly visualize the electrostatic field inside a diagnosed space that can be empty or occupied. The electric-field images are taken using a broadband, polarized neutron beam with a sensitive, transverse polarimetry scheme. This work may enable new diagnostic power of the structure of electric potential, electric polarization, charge distribution, and dielectric constant inside an investigated target by visualizing spatially dependent electric field from a distance.

Non-destructive but penetrative imaging technologies are powerful diagnostic tools, because they can reveal the structure of specific information inside diagnosed objects or subjects that cannot be easily observed or measured externally. Nowadays, these kinds of visualization technology have been broadly utilized in areas of medical exams, scientific researches, engineering trouble shootings, security applications, etc., and it will be highly beneficial to continuously develop new imaging diagnostic technologies. One of the advantageous imaging capabilities that has been long pursued but very challenging is the visualization of static electric-field (E-field) distributing over a targeting space, especially when it is physically isolated or occupied and cannot be reached by physical probes. With or without the externally applied electric field, the E-field information from the diagnosed target can be used to reveal spatially dependent electrostatic characteristics, such as electric potential, electric polarization, charge distribution, and dielectric constant, which are highly valuable for studies of material properties and physical structure; for examinations of electronic components and enclosed electronics; and for applications of security screening.

To date, the priorly demonstrated and proposed approaches of static E-field imaging use physical sensors of electric potential or sensors of electric field based on field effect transistors [1, 2], electro-optic effect [3], Kerr effect [4], and Rydberg atoms [5]. Therefore the electric field can be mapped out over the sensor locations. Apparently this approach does not work for the occupied or physically isolated space. Some inverse-problem solutions may help to determine the electric field away from the sensor locations. Unfortunately, the inverse problems of electric field are mostly ill-posed [6], and therefore the E-field imaging based on physical sensors is restricted within the free space around the sensor locations and the imaging resolution is limited by the distance from the imaging target to the sensors [1, 2, 7]. Hence, the previously demonstrated images are mainly E-field surveys near the surface of the diagnosed objects. In addition, owing to the technical difficulty of making a high-density, two-dimensional (2D) array of E-field sensors, a scanning scheme with single sensor or a 1D sensor array was usually used to obtain a full image [2, 8, 9].

To overcome the natural limitation of sensor-based E-field imaging, a novel approach is to send specific agents to directly interact with the electric field, and the agents can carry the E-field information to arrive the detector. From this perspective, neutrons can be a good candidate of the E-field probing agents [10], since they have good penetration capability through many materials especially metals and can interact with electric field while they are moving due to the effect of special relativity. In this paper, we show images of electrostatic field for first time using polarized neutrons. Our work may initiate a new avenue in imaging diagnostic technology.

The underlying physics of neutron E-field imaging is based on the neutron spin precession when neutrons are moving through a region of electric field. Neutron carries non-zero magnetic moment that is aligned to its spin orientation. The well-known dynamic of the spin precession is described by

$$\frac{d}{dt}\langle \mathbf{I}\rangle = \gamma_{\rm n}\langle \mathbf{I}\rangle \times \mathbf{B}_{\rm eff}, \tag{1}$$

where $\langle \mathbf{I}\rangle$ is the ensemble average of the neutron spin vector, $\gamma_{\rm n} = -1.83\times10^{8}$ rad s^{-1} T^{-1} is the gyromagnetic ratio of neutron, and the effective magnetic-field (B-field) vector seen by a moving neutron is

$$\mathbf{B}_{\rm eff} = \mathbf{B} - \frac{\mathbf{v}\times\mathbf{E}}{c^2}, \text{ for } |\mathbf{v}| \ll c. \tag{2}$$

Here, $\mathbf{B}$ and $\mathbf{E}$ are the spatially dependent B-field and E-field vectors in the laboratory frame, $\mathbf{v}$ is the velocity vector of the moving neutron, and c is the speed of light. Using Eq. (1) and Eq. (2), we find a net change in angle vector of a neutron spin due to field-induced precession from its trajectory l to be

$$\boldsymbol{\theta} = \int_l \frac{d\langle \mathbf{I}\rangle}{|\langle \mathbf{I}\rangle|} = \int_l \gamma_{\rm n}\left[\mathbf{e}_{\rm I}\times\frac{\mathbf{B}}{|\mathbf{v}|} - \mathbf{e}_{\rm I}\times\frac{(\mathbf{e}_v\times\mathbf{E})}{c^2}\right] dl, \tag{3}$$

Sandia National Laboratories is a multimission laboratory managed and operated by National Technology & Engineering Solutions of Sandia, LLC, a wholly owned subsidiary of Honeywell International Inc., for the U.S. Department of Energy's National Nuclear Security Administration under contract DE-NA0003525.

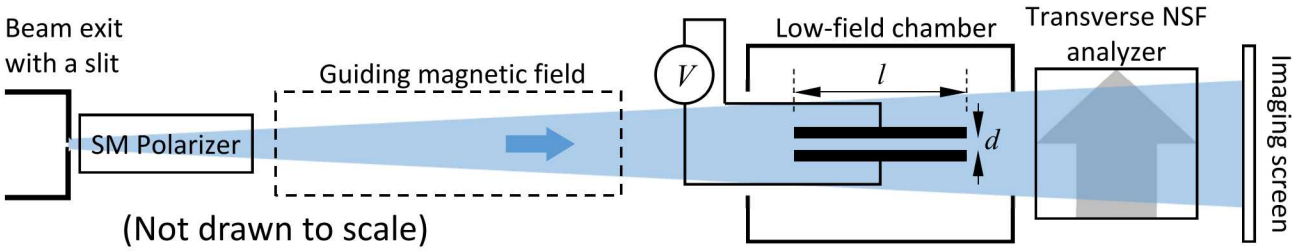

FIG. 1. A schematics of the E-field imaging experiments with polarized neutrons. The blue small arrow represents the polarization of the neutron beam before arriving the E-field region, which is in between the two parallel electrodes driven by a voltage source. The gray big arrow denotes the analyzing direction of neutron spins at the NSF-based analyzer.

where $\mathbf{e}_{\rm I} = \langle \mathbf{I} \rangle / |\langle \mathbf{I} \rangle|$ is the unit vector of neutron spin, and $\mathbf{e}_v = \mathbf{v}/|\mathbf{v}|$ denotes the unit vector along the velocity direction. Hence, in practice, we can polarize neutrons to have most of their spins align to the same direction, and the polarization vector is $\mathbf{P} = 2\langle \mathbf{I} \rangle$. The B-field and/or E-field information then can be determined by measuring the rotation angle of the polarized neutron spins, $\boldsymbol{\theta} = \boldsymbol{\Delta}\mathbf{P}/|\mathbf{P}|$ through a neutron polarimetry method. In Eq. (3), we see that the E-field effect to the spin rotation is independent of neutron velocity, but the B-field effect is velocity dependent. Hence, unlike the B-field measurement, the E-field measurement is not affected by the velocity spread of neutrons when using a broadband beam. Mathematically, we can engage different neutron velocities, different probing trajectories, different polarization orientations, and different analyzing directions to retrieve full vector information of both magnetic field and electric field. When electric field is the only interesting quantity in the measurement, we can in principle use very fast neutrons to minimize the effect from magnetic field.

There were demonstrations of B-field imaging based on neutron spin rotation signals [11, 12] but no E-field imaging was proposed or demonstrated before. One major challenge of detecting electric field with polarized neutrons is the much smaller induced spin rotation angle $\theta_{\rm E}$, which is generally $\ll 1$ rad due to the very small factor of $1/c^2$ in Eq. (3). On the other hand, the B-field induced rotation angle $\theta_{\rm B}$ can easily achieve > 1 rad in many experimental circumstances. Thus, in order to detect the E-field signals and produce E-field images, a neutron polarimetry method with high sensitivity of spin rotation angle is desired. In our neutron E-field imaging experiments, we incorporated our previously developed transverse neutron polarization analysis scheme with an angular resolution $\ll$ mrad (10^{-3} rad) [13] into a neutron imaging setup to visualize the electrostatic field produced inside experimental samples.

We conducted experiments of neutron E-field imaging using the NG6e (Neutron Guide 6 end station) [14] beamline at the U.S. National Institute of Standards and Technology (NIST) Center for Neutron Research (NCNR). An experimental diagram is sketched in Fig 1. Unpolarized polychromatic neutrons, covering wavelengths from 0.2 nm to 0.6 nm, that left the beam exit and passed a slit were polarized by a super-mirror (SM) polarizer. The polarized neutrons were then adiabatically transferred into the guiding field at about 1 mT (10 G) with polarization along the longitudinal direction (beam direction). The polarized neutrons maintained most of their polarization and entered a low-field chamber made by μ-metals with internal longitudinal B-field strength < 10 μT (0.1 G) and transverse B-field strength < 1 μT (10 mG). Inside the low-field chamber, there was a capacitor-like E-field sample with two parallel electrodes connected to a low-current, high-voltage (HV) source via HV cables. The electric field was produced in the region between the two parallel electrodes. Using Eq. (3), we find the total spin precession angle through the E-field region to be

$$\theta_E = \gamma_n \kappa E l / c^2, \tag{4}$$

where l is the length of the electrodes, and κ is the correction factor that is slightly greater than one due to the fringe E-field caused by the finite length l. Here the electric-field amplitude $E = V/d$ is defined by the driving voltage V across the parallel electrodes and the spacing d between the electrodes. The primary reason of placing the E-field sample inside a low-field chamber was for minimizing the spin precession due to the background B-field. This is important when using the cold neutron beam on NG6e for E-field imaging with slow neutron velocity ~ 1000 m/s. We used a transverse polarization analysis scheme with a neutron spin filter (NSF) based on polarized ^{3}He [13] as shown in Fig. 1 to provide spin-angle-dependent neutron intensity $I(\theta) \propto N_0(1 + \overline{P_{\rm n} A} \sin\theta)$ [13] on a 300 μm thick imaging screen that was made of LiF:ZnS. Here, N_0 is the detected neutron number within a given area on the screen, $\overline{P_{\rm n} A} \leq 1$ is the averaged product of the neutron polarization $P_{\rm n}$ and the analyzing power A for different neutron wavelengths in a polychromatic beam, and $\theta = \theta_E + \theta_B$. In this experiment, the $\theta_B \ll 1$ can be treated as a constant background. For $\theta \ll 1$, we find the E-field signal contrast

$$\frac{I(\theta_E + \theta_B) - I(\theta_B)}{I(\theta_B)} = \overline{P_{\rm n} A} \theta_E. \tag{5}$$

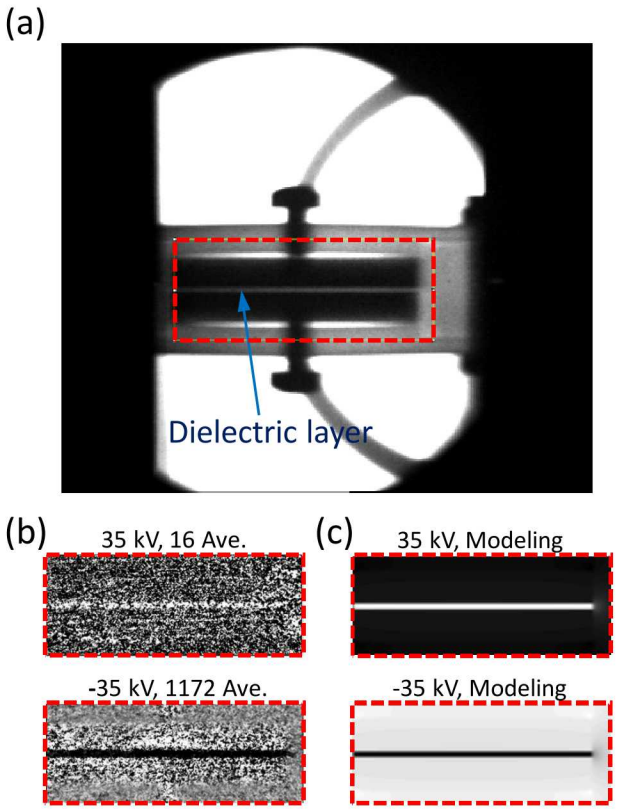

FIG. 2. (a)Normal neutron image of the short-version E-field sample. (b) Electric-field images from the dashed-line selected area in (a) with two different statistics and two driving voltages at 35 kV and -35kV on the E-field sample. (c) Modeling results of the polarized neutron E-field images for the same field of view.

The LiF:ZnS screen generates scintillated photons that are proportional to the neutron intensity for optical imaging. In the E-field imaging experiments, we set the slit width to be 11 mm at the beam exit. The distances from the E-field sample to the beam exit and to the imaging screen were about 7 m and 55 cm. The vertical imaging resolution was then about 0.9 mm. More detailed information regarding the NG6e beamline, the experimental components, and the transverse polarimetry scheme used in this work can be found in Ref.[13].

In this proof-of-concept experiments, we imaged two E-field samples (long and short versions). The body of the E-field samples were made of perfluoroalkoxy (PFA) due to the reasons of relatively high neutron transmission and high dielectric strength. The rectangular electrodes made of borated aluminum were enclosed inside the machined PFA body separated by a PFA membrane as the dielectric layer. In the long-version sample, the electrodes were 5 cm wide, $l = 11.4$ cm, and 6.35 mm thick, and the electrode spacing $d = 400 \pm 50$ μm. In the short-version sample, the electrodes were 5 cm wide, $l = 5.7$ cm, and 6.35 mm thick, and the electrode spacing $d = 500 \pm 50$ μm. In Fig. 2, we present some experimental images and the modeling results. Figure 2a is a normal neutron image of the short-version E-field sample. The two rectangular, black areas at the center are the two electrodes. The PFA dielectric layer in between the electrodes can be clearly seen. From this image, we can also see some nylon screws and the two HV cables. The usable imaging area was defined by the opening window on the NSF analyzer with two straight-line boundaries on the sides and curved boundaries on the top and bottom. When doing the E-field imaging, we sequentially took images with the HV source alternating between the ON and OFF states. Each image was the result of the median combination of 3 frames, with a frame exposure time of 45 s. Since the PFA material and the plastic screws in the E-field sample produced scattered neutrons that can impact the quality of E-field image, we used a borated mask placed right before the low-field chamber to minimize the volume of the sample that was exposed to the neutron beam for reducing the scattered neutrons. The mask had a rectangular opening, and the field of view was then defined by the area selected by the dashed line in Fig. 2a. To produce the E-field image, we generated a contrast image by performing (I(ON)−I(OFF))/I(OFF) from each image pair as indicated in Eq. (5). Here, I(ON) and I(OFF) denote the images with the HV source ON and OFF. We then averaged all the contrast images to obtain better statistics. Figure 2b presents two E-field images of the short-version E-field sample at 35 kV supplied voltage with 16 averages and at -35 kV supplied voltage with 1172 averages. Since reversing driving voltage also change the sign of the electric field and therefore change of the sign of θ_E, we then see the bright and dark responses on the images. Figure 2c illustrates the modeling results of the same conditions and field of view with an assumption of uniform neutron flux. We can see qualitative agreements between the experimental and the modeling images.

From a practical point of view, the E-field state in a diagnosed sample is usually not externally adjustable. A preferable way of imaging E-field would be taking two images with two opposite directions of neutron polarization with a fixed analyzing direction or taking the images with two opposite analyzing directions with fixed neutron polarization to generate an image pair with opposite θ_E in the measurements. Using this pair of images, we will obtain a contrast image with 2x amplitude on the imaging areas that have non-zero spin precession angle caused by the E-field. In this work, we did not implement the capability of spin flipping to the polarized, polychromatic neutron beam or to the NSF analyzer. Therefore, we actively switched the E-field at ON and OFF states for demonstrating E-field images.

To verify the responses of the electric field to the images, we measured the signal contrasts from the dielectric area on the images with several driving voltages from −35 kV to 35 kV on the short-version sample; 36kV on

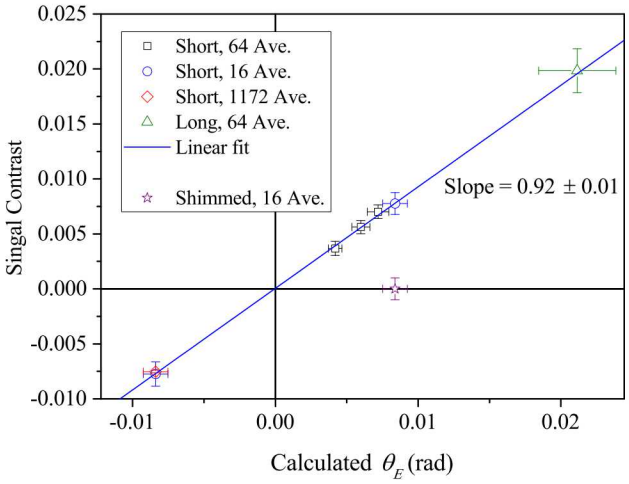

FIG. 3. E-field signal contrasts vs the calculated θ_E. "Short" and "Long" represent the data points from the short-version and long-version E-field samples. "Shimmed" represents the data point using depolarized neutrons.

the long-version sample; and 35kV on the short-version sample with a shimmer (neutron depolarizer) in front of the sample. Figure3 plots the measured signal contrasts versus the calculated $\theta_E = \gamma_n \kappa V l / dc^2$. From the finite element modeling (FEM), we found $\kappa \approx 1.032$ for the short-version sample and $\kappa \approx 1.014$ for the long-version sample. From Eq. (5), the slope of the fitting line gives $\overline{P_n A} = 0.92 \pm 0.01$, which is within the range of the typically expected values from our polarimetry setup. We see zero signal contrast with the shimmed case as a proof of the need of polarized neutrons for E-field imaging. In Fig. 3, the horizontal error bars are mainly attributed to the machining uncertainty on the PFA membrane thickness, which is ± 50 μm, and the vertical error bars are limited by the imaging statistics. The neutron transmission is about 10.5% through the short-version sample and 1.6% through the long-version sample. With the short-version sample, the detected neutron flux rate on the imaging screen was about 10^3 n cm^{-2} s^{-1} in the dielectric area based on the gray-value readings on the image. In the experiments, the E-field image with the best statistics is the -35 kV driving voltage on the short-version sample with 1172 averages of the contrast images. Using the entire E-field signal area (about 5 cm by 1 mm), we find its measurement uncertainty is about 1.5% as shown in Fig. 3. The shot-noise-limit angular resolution $\delta\theta$ of the neutron spin precession can be calculated by $1/\overline{P_n A} N_0^{1/2}$ [13, 15]. We find N_0 = (neutron flux rate)×(area)×(frame number)×(exposure time)×(image number)= $10^3 \times 0.5 \times 3 \times 45 \times 1172$ = 79,110,000. Hence, $\delta\theta = 0.12$ mrad. The $|\theta_E|$ from -35kV on the short-version sample is -8.4 mrad. We then find $\delta\theta/|\theta_E| = 1.4\%$, which is pretty close to the measured uncertainty. Hence, the minimally detectable voltage on the short-version sample is about 500 V using the 1172-averaged contrast images.

Considering an achievable experimental setting with a total detected neutron flux of 10^{12} n cm^{-2}. We find that the minimally detectable E-field strength in 1 cm^3 volume to be about 5×10^4 V/m (equivalent to 500 V across 1 cm distance) and in 1 mm^3 volume to be about 5×10^6 V/m (equivalent to 5000 V across 1 mm distance). We believe this kind of E-field sensitivity is sufficient for several image diagnostics applications with investigated targets, such as high-voltage electronics, which usually has capacitors with internal E-field strengths $> 10^7$ V/m, dielectric materials with externally applied very high E-field, and ferroelectric materials, which usually have spontaneous electric polarization with equivalent E-field strength $> 10^8$ V/m.

We have demonstrated direct images of electrostatic field of the E-field samples using a polarized, polychromatic neutron beam. Before this work, visualizing electric field inside a diagnostic space that is occupied was not feasible. In addition, owing to the great penetration capability of neutrons through metals, this neutron E-field imaging technology can also measure the electric field that is inside a shielded space, which cannot be achieved by any other existing technology. Our work may enable new diagnostic power of the structure of electric potential, electric polarization, charge distribution, and dielectric constant inside an investigated target by visualizing spatially dependent electric field from a distance.

This work was supported by the Laboratory Directed Research and Development program at Sandia National Laboratories. Sandia is a multimission laboratory managed and operated by National Technology and Engineering Solutions of Sandia (NTESS), LLC, a wholly owned subsidiary of Honeywell International Inc., for the U.S. Department of Energy National Nuclear Security Administration under contract DE-NA0003525. We acknowledge the support of the National Institute of Standards and Technology, US Department of Commerce, in providing the neutron facilities used in this work. The NIST effort was partially supported by the U.S. Dept. of Energy, Office of Nuclear Physics, under Interagency Agreement 89243019SSC000025. This paper describes objective technical results and analysis. Any subjective views or opinions that might be expressed in the paper do not necessarily represent the views of the U.S. Department of Energy or the United States Government.

* Corresponding author: yjau@sandia.gov

[1] W. Gebrial, R. J. Prance, C. J. Harland, and T. D. Clark, Rev. Sci. Inst. **77**, 063708 (2006).
[2] E. R. Generazio, AIP Conf. Proc. **1806**, 020025 (2017).
[3] Y. Zhut, T. Takadat, and D. Tu, J. Phys. D: Appl. Phys. **28**, 1468 (1995).

[4] M. Zahn, IEEE Trans. Diel. Elec. Insu. **1**, 235 (1994).

[5] Y.-Y. Jau and T. Carter, Phys. Rev. Applied **in press** (2020).

[6] S. I. Kabanikhin, J. Ivn. Ill-Posed Problems **16**, 317 (2008).

[7] S. T. Beardsmore-Rust, P. Watson, R. J. Prance, C. J. Harland, and H. Prance, Meas. Sci. Technol. **20**, 095711 (2009).

[8] R. J. Prancey, T. D. Clarkz, H. Prance, and A. Clippingdale, Meas. Sci. Technol. **9**, 1229 (1998).

[9] W. Gebrial, R. J. Prance, T. D. Clark, C. J. Harland, H. Prance, and M. Everitt, Rev. Sci. Inst. **73**, 1293 (2002).

[10] Y.-Y. Jau, (2018), a research proposal, Sandia National Laboratories.

[11] M. Dawson, I. Manke, N. Kardjilov, A. Hilger, M. Strobl, and J. Banhart, New J. Phys. **11**, 043013 (2009).

[12] M. Strobl, N. Kardjilov, A. Hilger, E. Jericha, G. Badurek, and I. Manke, Physica B **404**, 2611 (2009).

[13] Y.-Y. Jau, W. Chen, T. Gentile, and D. Hussey, Rev. Sci. Inst. **submitted** (2020).

[14] D. Hussey, C. Brocker, J. Cook, D. Jacobson, T. Gentile, W. Chen, E. Baltic, D. Baxter, J. Doskow, and M. Arif, Physics Procedia **69**, 48 (2015).

[15] W. M. Snow, E. Anderson, L. Barrn-Palos, C. D. Bass, T. D. Bass, B. E. Crawford, C. Crawford, J. M. Dawkins, D. Esposito, J. Fry, H. Gardiner, K. Gan, C. Haddock, B. R. Heckel, A. T. Holley, J. C. Horton, C. Huffer, J. Lieffers, D. Luo, M. Maldonado-Velàzquez, D. M. Markoff, A. M. Micherdzinska, H. P. Mumm, J. S. Nico, M. Sarsour, S. Santra, E. I. Sharapov, H. E. Swanson, S. B. Walbridge, and V. Zhumabekova, Rev. Sci. Instrum. **86**, 055101 (2015).